CIRP Journal of Manufacturing Science and Technology 59 (2025) 118–126

Contents lists available at ScienceDirect

CIRP Journal of Manufacturing Science and Technology

journal homepage: www.elsevier.com/locate/cirpj

Advanced ultra-high precision system (NanoCyl) for accurate cylindricity measurements

Rim Bennoune [a,e,*], Gengxiang Chen [d], Saint-Clair Toguem Tagne [a], Alain Vissiere [a], Mohamed Damak [b,c], Charyar Mehdi-Souzani [d], Nabil Anwer [e], René Mayer [f], Hichem Nouira [a]

[a] Laboratoire Commun de Métrologie, Laboratoire National de Métrologie et d'Essais (LNE-CNAM), 1 Rue Gaston Boissier, 75015 Paris, France
[b] GEOMNIA, 19B rue des Châteaux, 59290 Wasquehal, France
[c] Arts et Métiers Institue of Technology, LISPEN, 8, Bd Louis XIV, 59046 Lille Cedex, France
[d] Université Paris-Saclay, Université Sorbonne Paris Nord, ENS Paris-Saclay, LURPA, 91190 Gif-sur-Yvette, France
[e] Université Paris-Saclay, ENS Paris-Saclay, LURPA, 91190 Gif-sur-Yvette, France
[f] Polytechnique Montreal, Montréal, QC H3T 1J4, Canada

ARTICLE INFO

Keywords:
Measuring machine
Ultra-high precision
Traceability
Data processing

ABSTRACT

Achieving ultra-high precision in manufacturing relies on accurate measurement systems, especially for geometries like cylindricity, which are fundamental components for precision engineering. However, current commercial cylindricity measuring machines struggle to provide the required ultra-high precision or comprehensive error analysis. This work develops an ultra-high precision cylindricity measuring machine (NanoCyl) for cylindricity profile extraction and accurate defect assessment with nanometre uncertainty. The NanoCyl incorporate the dissociated metrology structure and strict adherence to the Abbe principle, ensuring unparalleled accuracy by minimising external and internal disturbances. With in-situ calibration of capacitive probes and advanced data processing, the NanoCyl maintains traceability to the SI metre to ensure the high-precision performance. Error separation techniques (EST) are integrated into the NanoCyl to further eliminate the machine axis errors and optimise the measurement uncertainty. The NanoCyl can evaluate the three main components of cylindricity, as defined by ISO 12180–1: cross-section deviations through EST, median line deviations from harmonic signal analysis, and radial deviations using synchronised measurements from opposite probes. Experimental validation demonstrates the NanoCyl's capability to achieve a standard measurement uncertainty within a few tens of nanometres. These findings highlight its potential for significantly improving the accuracy of cylindricity measurements, ensuring better quality control in high-precision manufacturing.

1. Introduction

Cylindrical features are essential components used in most mechanical devices such as rolling bearings, machine tool spindles, engine pistons and shafts, manometers, piston-cylinder assemblies, etc. Form errors of cylindrical features can significantly influence both the performance and lifetime of mechanical devices. To achieve submicrometre form error and nanometre roughness, precision machining is usually combined with in-situ and offline ultra-high accuracy metrology and robust traceable software in an iterative manufacturing process chain as specified in Fig. 1 [1–5]. Pre-manufacturing (milling, grinding, etc.) (2) of canonical and complex axisymmetric CAD modelled features (1), followed by a coarse measurement (3), is initially performed. The following step is an iterative process starting with a multi-axis computer numerical control (CNC) diamond turning (4). The resulting features are measured in-line using tactile or optical in-situ measuring devices (5) and analysed through validated data post-processing software (6). The detected deviations are corrected in an iterative machining process followed by accurate offline measurements (7). The iterative machining process is performed until the desired shape tolerance (8) is reached and surface texture sufficiently approached. The traceability of the coarse (3), in-situ (5) and offline measuring instruments (7) achievable with an ultra-high precision measuring instrument (9) combined with advanced robust software (10) is a critical

* Corresponding author at: Laboratoire Commun de Métrologie, Laboratoire National de Métrologie et d'Essais (LNE-CNAM), 1 Rue Gaston Boissier, 75015 Paris, France.
E-mail addresses: rim.bennoune@lne.fr (R. Bennoune), hichem.nouira@lne.fr (H. Nouira).

https://doi.org/10.1016/j.cirpj.2025.03.005
Received 5 December 2024; Received in revised form 4 March 2025; Accepted 15 March 2025
Available online 26 March 2025

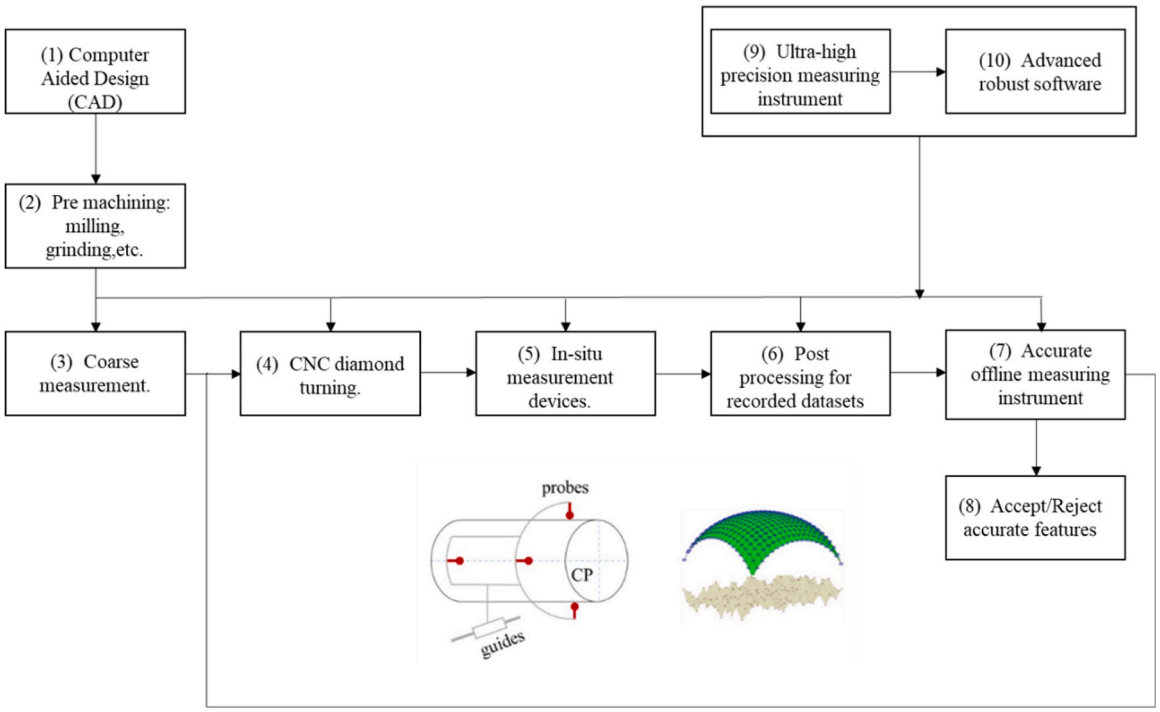

Fig. 1. Iterative process chain for ultra-accurate manufacturing.

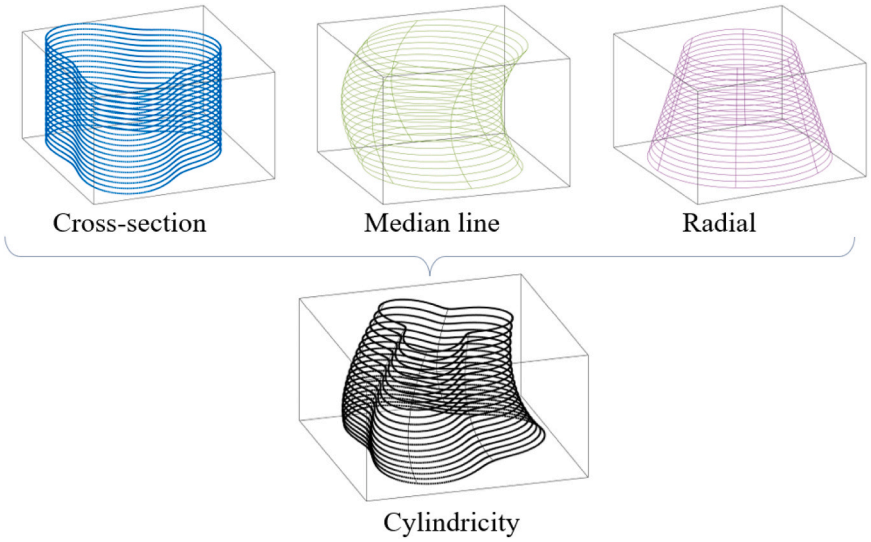

Fig. 2. Elements of cylindricity deviations as defined in ISO 12180–1 [6].

requirement in the iterative process chain to optimise the number of iteration for rapid tolerance achievement.

According to ISO 12180–1 [6], cylindricity deviations are attributed to three simple independent elements: (1) cross-section deviations, (2) radial deviations and (3) median line deviations as illustrated in Fig. 2. In basic applications the cylindrical part (CP) median line deviations and radial deviations are assumed to be low compared to cross-section deviations. When an ultra-high accuracy measurement of the cylindricity error is required, both radial and CP median line deviations are estimated from the measurements of sets of opposite generatrixes. The cylindricity deviations are then calculated by combining the obtained median line deviations with the cross-section deviations. Although this method of approximating the cylindricity deviations is described in the ISO 12180–1 [6], practical difficulties remain in accurately identifying the various elements of cylindricity deviations with commercial cylindricity-measuring machines used in industrial inspection laboratories [3].

As reported by the Bureau International des Poids et Mesures (BIPM), most published calibration and measurement capabilities (CMCs) in cylindricity assessment using commercial machines have uncertainties higher than 200 nm for medium scale CPs of a few hundred millimetres diameter and length. In the case of large CPs, the best achievable uncertainty is in the order of a micrometre [7–9].

The ultra-high precision measuring machine, NanoCyl, designed for calibrating CPs and piston-cylinder assemblies with low uncertainty, is detailed in Section 2. The strategy for analysing the measurement data is presented in Section 3, with the cylindricity measurement results and their associated uncertainty discussed in Sections 4 and 5, respectively.

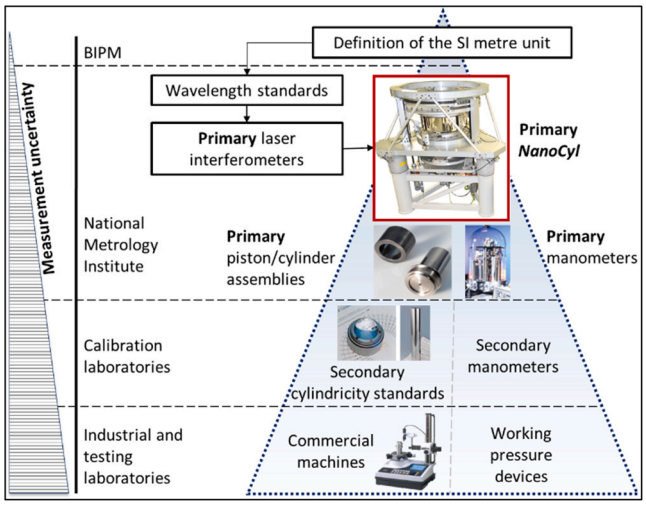

Fig. 3. Established traceability for cylindricity measurements for piston-cylinder assemblies and material CP transfer standards.

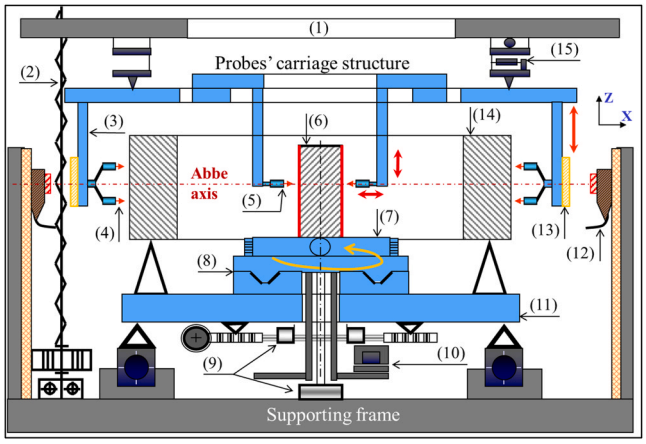

Fig. 4. Architecture of the primary NanoCyl applying the Precision Design Principles [15]: (1) XY translation table, (2) linear guidance, (3) metrology frame, (4) reference probes, (5) measuring probes, (6) cylindrical part, (7) automated tilt/centre table, (8) rotary indexing table, (9) encoders, (10) brake, (11) rotary table, (12) laser interferometers, (13) reflective mirror, (14) reference cylinder, (15) piezoelectric actuators.

2. Design of the ultra-high cylindricity measuring machine (NanoCyl)

NanoCyl design is based on a rigorous application of precision design principles (PDPs), such as the use of a metrology frame, which aim at minimising interferences for minimal measurement uncertainties [10, 11]. The traceability of NanoCyl to the SI definition of the metre unit is achieved by means of calibrated laser interferometers. Its purpose is to provide:

- Metrological traceability of material transfer standards used in the qualification of industrial roundness machines (Fig. 3),
- Ultra-high accuracy calibration of cylindrical features in extremely demanding fields such as high surface quality of piston-cylinder assemblies integrated into primary manometric balances for pressure metrology.

The architecture of the NanoCyl, illustrated in Fig. 4, applies the dissociated metrology technique (DMT), by using two distinct frames: a metrology frame and a structural frame. The metrology frame includes

Table 1
Technical characteristics of the sensors.

Capacitive sensor model	MCC10 (Fogale)
Measurement Range	500 µm
Resolution	0.1 nm
Non-linearity error	< 0.05 %
Sensitive Surface Diameter	10 mm
Laser interferometer	**RLE20 (Renishaw)**
Frequency stability	< ±1 ppb (1 min)
Thermal drift coefficient	< 50 nm/°C
Non-linearity error:	< ±1 nm
Electrical noise	< 0.2 nm RMS

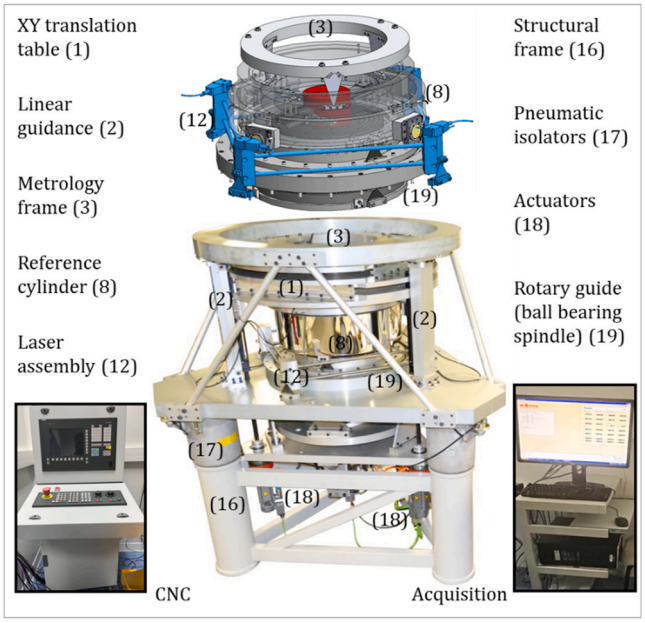

Fig. 5. Architecture of the primary NanoCyl applying the PDPs [15]: (1) XY translation table, (2) linear guidance, (3) metrology frame, (4) reference probes, (5) measuring probes, (6) CP, (7) automated tilt/centre table, (8) rotary indexing table, (9) encoders, (10) brake, (11) rotary table, (12) laser interferometers, (13) reflective mirror, (14) reference cylinder, (15) piezoelectric actuators.

the CP (6) and the reference cylinder (14) mounted on the rotary table (11) driven by a precision ball-bearings spindle. Isostatic linkages (flexible blades) are used for fixing the rotary table on the ball-bearings spindle. Similarly, isostatic linkages are also used for fixing the reference cylinder on the rotary table. It leads to exact-constraint connections and thermally isolate the reference cylinder from heat sources such as friction in rotary and linear motion stages. The vertical positioning of the probes' carriage structure (with reference (4) and measuring (5) capacitive probes) is carried out with three synchronised linear stages (2) using a computer numerical control (CNC) under the control of linear optical encoders with micrometric accuracy. Two angular encoders (9) are embedded in the rotary table allowing a precise acquisition (resolution of 0.02°) of the angular positions of the CP and of the reference cylinder. The rotary indexing table (8) and the brake (10) are used when applying any error separation technique (reversal and/or multi-step [12–14]) requesting angular shifting of the CP with respect to the reference cylinder. An additional high-precision tilt/centre mechanism (7) is fixed on the rotary table to perform accurate alignment of the CP axis with the rotational axis of the NanoCyl. It provides four degrees of freedom (x- and y-translation as well as x- and y-rotation) using only flexible blades.

The probes' carriage structure (3) is equipped with four reflective mirrors (13) made of Zerodur® material on which four laser

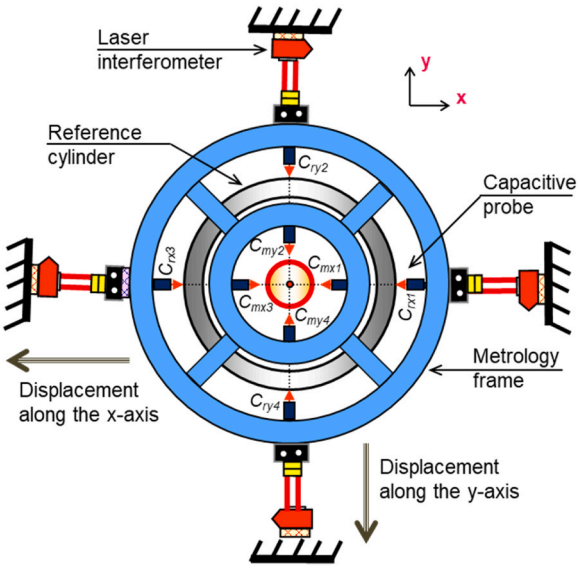

Fig. 6. Calibration of Capacitive Probes using laser interferometers [15].

interferometers (12) are aligned. They are necessary for achieving in-situ calibration of both the reference (4) and the measuring probes (5) while respecting the Abbe principle [16]. Once the measuring or reference probes have been aligned along the Abbe axis, passing through two opposite laser interferometers, the calibration is carried out by translating the probes' carriage structure (3) with an XY translation Table 1. The latter uses two perpendicular piezoelectric actuators (15) and four flexible blades to perform linear motions over an 80 µm range. Each probe reading is compared to the displacement recorded by the two laser interferometers. The wavelength calibration of the lasers allows the measurements to be traceable to the fundamental SI definition of the metre unit. The in-situ calibration of the sensitive probes of the NanoCyl drastically reduces the effects of positioning errors, form shape of the CP and relative orientation [17].

One advantage of the application of the DMT is the possibility to design the high-precision NanoCyl with axial symmetry (Fig. 4 and Fig. 5), where the form of the CP is compared to that of the reference cylinder. All mechanical parts are made of aluminium. The metrology performance of the NanoCyl is not limited by the motion errors of the ball bearing spindle and the mechanical linear guidance as for classical measurement machines. Only the performances of both the measuring probes (C_m) and the reference probes (C_r) in particular their random errors and non-linearities [15], are critical. Random errors are mitigated with spatial and temporal redundancies by aligning eight capacitive probes on the reference cylinder and four capacitive probes on the CP as well as by multiplying the number of measurements. Furthermore, the application of the DMT leads to reducing the NanoCyl sensitivity to internal and external disturbances since the metrology frame is dissociated from the structural frame through isostatic mechanical linkages [11] (e.g., flexible blade). The detailed specifications of the sensors are listed in Table 1.

The architecture of the NanoCyl is symmetric along the z-axis, which provides a flexibility in the selection of materials. Therefore, 95 % of mechanical parts are made of aluminium material to cope with the adopted dissociated metrology technique (DMT). Aluminium presents a high thermal expansion coefficient, and also a high diffusivity parameter that leads to correct measurements by investigating opposite capacitive probes.

3. In-situ calibration of capacitive probes

Measurement uncertainty in ultra-high precision instruments often arise from errors in probe positioning, alignment and non-linearity. Since the cylindricity measurement target an accuracy few tens of nanometres, in-situ calibration of the capacitive probes with regards to the reference cylinder and cylindrical part is adopted for the NanoCyl, while minimising established errors.

The calibration process begins with the pre-alignment of two opposite capacitive probes to two laser interferometers positioned along the same horizontal reference measurement axis (Fig. 6), while respecting the Abbe principal with a positioning error less than 20 µm. Once the two capacitive probes are pre-aligned, in-situ calibration is performed at the probe's operating range. This approach is central to the NanoCyl system, as it allows for the correction of non-linearity errors directly in the system. Zerodur mirrors, known for their excellent thermal stability ($\alpha_{Zerodur} \approx 0.01 \times 10^{-6}\ K^{-1}$), are clumped on the XY carriage structure made of aluminium ($\alpha_{aluminium} \approx 0.01 \times 10^{-6}\ K^{-1}$) alongside the capacitive probes. Even if the expansion coefficients are not similar, the impact of the smooth variation of the temperature in the controlled metrology room (20 °C) of $< 0.3°$ on the calibration range of < 100 µm is negligible (<0.5 nm).

The piezoelectric actuators integrated in the XY translation Table 1 control the displacements with an ultra-high precision. The laser interferometers are aligned with the Zerodur mirrors and positioned opposite the capacitive probes, ensuring that the displacements measured by the lasers directly correspond to the displacements perceived by the capacitive probes.

Laser interferometers serve as reference standards for displacement measurements. These provide high-accuracy measurements traceable to the SI metre definition. During the in-situ calibration, the displacement detected by the capacitive sensors (in volts) is compared with the

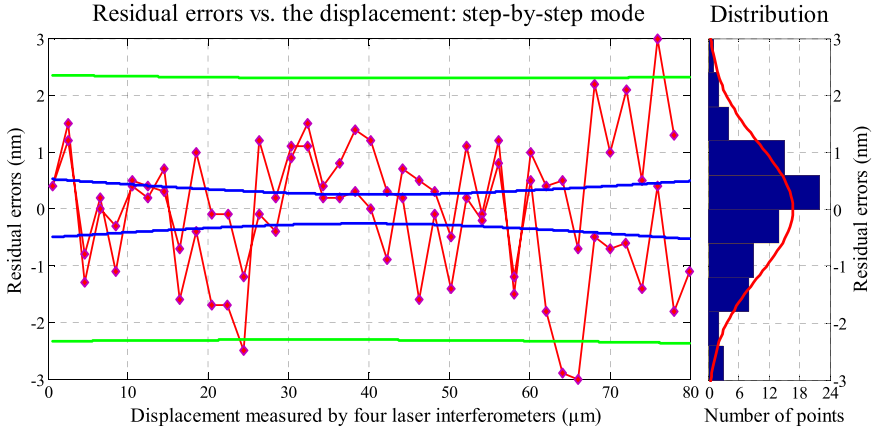

Fig. 7. Step by step calibration of one capacitive probe, third-order polynomial fitting model.

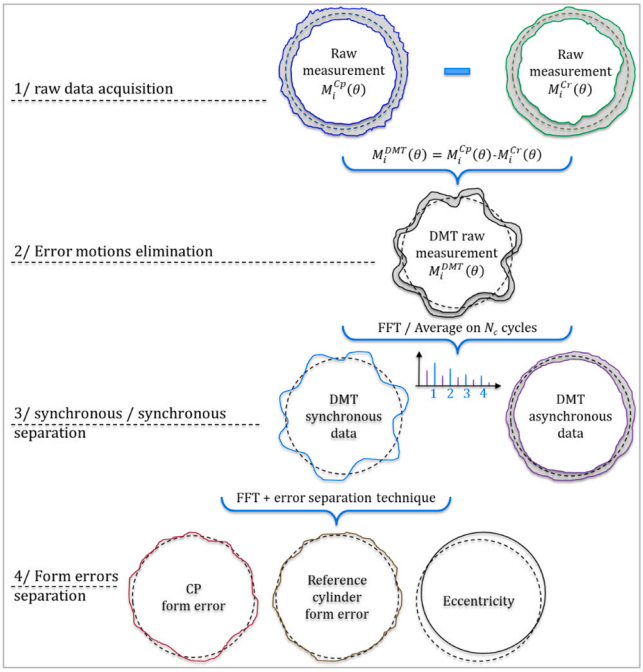

Fig. 8. Schematic diagram of the processing strategy.

displacement measured by the laser interferometers (in nanometres). Both systems operate synchronously to capture displacement data, ensuring accurate alignment between the measurements. This reduces discrepancies caused by misalignments or environmental factors that might affect the probes during calibration.

One significant advantage of the in-situ calibration is its ability to correct sensor non-linearity, which arises from non-uniform electric fields, particularly when the probe's target surface is not flat. In-situ calibration corrects these non-linearities, thereby improving measurement accuracy. The result is that any positioning and alignment errors are reduced to the calibration uncertainty, as characterised by the residuals of the calibration process (Fig. 7). The residual errors observed during the calibration process confirm the precision and reliability of the methodology. In the step-by-step calibration approach, errors were confined to ± 2 nm over an 80 μm travel range using a third-order polynomial fitting model. It demonstrates the method's effectiveness in addressing systematic deviations. Similarly, continuous calibration yielded comparable residual errors, particularly when averaging over 100 data points, proving its robustness for real-time operational calibration.

4. Analysis of DMT measurement datasets

The process for extracting synchronous components and estimating cylindricity parameters follows a structured approach to refine the raw measurement data and correct for various errors. The process begins with pre-processing the raw data to separate synchronous and asynchronous components, addressing errors such as thermal drifts and vibrations. Next, the revisited reversal technique is applied to isolate the form errors of the reference cylinder and the measuring system (CP). Following this, median line deviations are calculated to align circularity profiles relative to the reference cylinder, isolating cross-sectional errors. Radial deviations are then determined by analysing measurements at specific points, while accounting for probe errors. Finally, cylindricity parameters are estimated through filtering, surface fitting, and calculating peak-to-valley deviations.

Each step in this process builds upon the previous one, ensuring a thorough and accurate analysis. The subsections that follow provide a detailed breakdown of each step in the analysis process, outlining the methodologies and calculations involved.

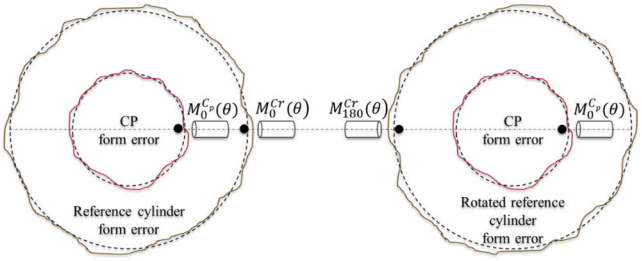

Fig. 9. Revisiting reversal error separation technique. M_0^{Cp} and M_{180}^{Cp} in the above text.

4.1. Extraction of the DMT synchronous components

Pre-processing the raw data is a prerequisite for extracting the synchronous repeatable components, defined in [18]. The synchronous/asynchronous separation is carried out on the DMT signal $M_i^{DMT}(\theta)$ resulting from the arithmetic combination of $M_i^{Cp}(\theta)$ and $M_i^{Cr}(\theta)$ roundness measurements for the CP and reference cylinder, respectively (Fig. 8). Assume that all capacitive probing systems are perfect, the application of the DMT leads to the suppression of the motion errors of the rotary table including both systematic and random errors. The DMT signal $M_i^{DMT}(\theta)$ contains components related to the CP form error, reference cylinder form error, eccentricity, thermal drifts, vibrations, frictions, etc.

Since the capacitive probes are calibrated in-situ, the nonlinear residuals errors are estimated below 5 nm and randomly distributed [15]. Thermal drifts, vibrations and frictions are asynchronous, while eccentricity corresponds to the first order of the DMT synchronous dataset. The synchronous/asynchronous separation allows the reduction of random and uncontrolled error effects on the measurements. The further challenge consists in separating the CP form errors from that of the reference cylinder, both combined in the DMT synchronous dataset, by applying a revisited reversal separation technique.

4.2. Revisiting reversal error separation technique for cross-section

The revisited reversal technique is inspired by the Donaldson reversal [11,16,18], applied on the DMT synchronous data (Fig. 8). The first step consists of performing simultaneous measurements of the CP $M_0^{Cp}(\theta)$ and reference cylinder $M_0^{Cr}(\theta)$ over a complete revolution (Fig. 9). The second step consists of carrying out an angular shift of the CP of 180° relative to the rotary table and reference cylinder from the initial position using the rotary indexing table. Then, additional simultaneous measurements of the CP $M_{180}^{Cp}(\theta)$ and the reference cylinder $M_0^{Cr}(\theta)$ are carried out over 360° of the rotary table. The synchronous radial error motions of the spindle are inversed by reversing the CP and exploiting the opposite measuring probes, as the *NanoCyl* is symmetric.

Let $m_i^{Cp,Cr,DMT}(\theta)$ be the synchronous components of the raw measurements data $M_i^{Cp,Cr,DMT}(\theta)$, $p(\theta)$ and $r(\theta)$ be the roundness of the CP and reference cylinder, and $B_{X_i}(\theta)$ the synchronous spindle error motions along the x-axis. In the absence of eccentricity errors (filtered with the first harmonic), the problem could be solved as follows:

$$m_1^{Cp}(\theta) = p(\theta, z) + B_{X_1}(\theta, z) \tag{1}$$

$$m_1^{Cr}(\theta) = r(\theta, z) + B_{X_1}(\theta, z) \tag{2}$$

$$m_0^{DMT}(\theta) = m_1^{Cp}(\theta) - m_1^{Cr}(\theta) = p(\theta, z) - r(\theta, z) \tag{3}$$

$$m_2^{Cp}(\theta) = p(\theta, z) - B_{X_2}(\theta, z) \tag{4}$$

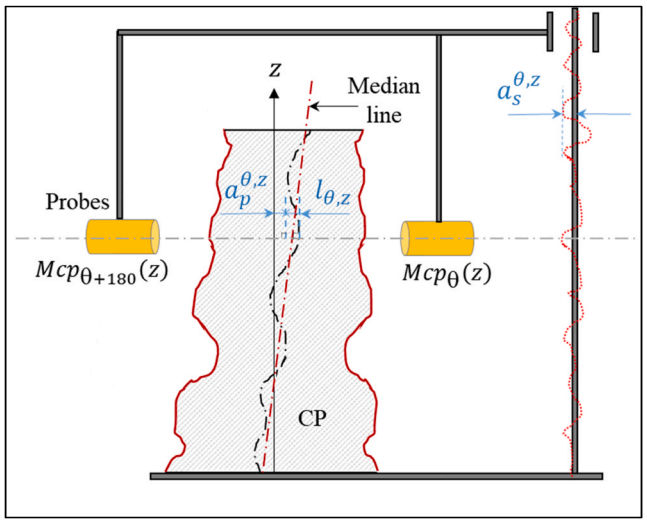

Fig. 10. Opposite probes for radial deviations detection.

$$m_2^{Cr}(\theta) = r(\theta,z) + B_{X_2}(\theta,z) \tag{5}$$

$$m_{180}^{DMT}(\theta) = m_2^{Cp}(\theta) + m_2^{Cr}(\theta) = p(\theta,z) + r(\theta,z) \tag{6}$$

$$p(\theta) = \frac{1}{2}\left(m_0^{DMT}(\theta) + m_{180}^{DMT}(\theta)\right) \tag{7}$$

$$r(\theta) = \frac{1}{2}\left(m_{180}^{DMT}(\theta) - m_0^{DMT}(\theta)\right) \tag{8}$$

The adopted revisited reversal error separation technique is applied at each cross-section and combined with a temporal repetition of the recordings over N_c cycles. The DMT synchronous components $m_i^{DMT}(\theta)$ are estimated by arithmetic average of the N_c cycles at each angular measurement location [14]. The measurement protocol is repeated at multiple vertical positions to cover the entire length of the CP.

4.3. Median line deviations

The median line deviations of the CP are calculated using the first harmonic of the DMT synchronous signal, which results in aligning the circularity profiles in the coordinate system of the reference cylinder. By referencing the position of each circularity profile to the first profile, we obtain their relative positions within the reference cylinder frame. This relative positioning is necessary, as it isolates only the cross-sectional circularity profiles in the reference coordinate system, focusing on their spatial alignment rather than absolute positioning, which helps identify median line deviations effectively.

4.4. Radial deviations

The radial deviations are calculated with at least four generatrixes at cardinal points (0°, 180° and 90°, 270°) when using opposite probes. In addition to the CP local form deviations $\vartheta(\theta,z)$, the probes recordings (Eqs. (9 and 10)) include radial deviations $r_d(\theta,z)$, median line deviations $l_{\theta,z}$, probes vertical error motions $a_s^{\theta,z}$ and CP alignment errors $a_p^{\theta,z}$ (Fig. 10).

$$Mcp_{\theta}(z) = \quad r_d(\theta,z) + \vartheta(\theta,z) - a_s^{\theta,z} - l_{\theta,z} - a_p^{\theta,z} \tag{9}$$

$$Mcp_{\theta+180}(z) = \quad r_d(\theta,z) + \vartheta(\theta+180,z) + a_s^{\theta,z} + l_{\theta,z} + a_p^{\theta,z} \tag{10}$$

The arithmetic average of these two opposite measurements along the generatrix at θ, $Mcp_{\theta}(z)$ and $Mcp_{\theta+180}(z)$, respectively, leads to the suppression of the median line deviations, the probes' vertical error motions and the CP alignment errors. The resulting linear arithmetic calculation (Eq. (11)) could be split into low integer harmonics (radial deviations $r_d(\theta,z)$) and high integer harmonic (residual form errors). A best estimate of the radial deviations could be achieved through several measurements performed in different generatrixes planes, and combined with harmonic FFT filtering. Alternatively, the residual local form errors can be attenuated by averaging over several recordings at different angular locations.

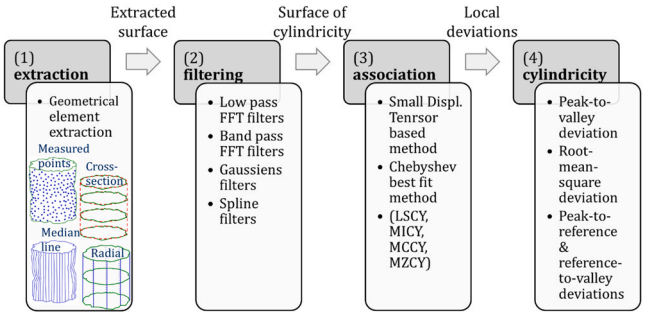

Fig. 11. Implemented strategy for evaluating the cylindricity, including the extraction and combination of the three elements (cross-section deviations, median line and radial deviations).

$$\frac{Mcp_{\theta}(z) + Mcp_{\theta+180}(z)}{2} = r_d(\theta,z) + \frac{\vartheta(\theta,z) + \vartheta(\theta+180,z)}{2} \tag{11}$$

4.5. Cylindricity parameters estimation

The NanoCyl allows extracting numerous cross-sectional profiles and identifying their relative locations (median line) in the reference coordinates system. The radial deviations are determined through several parallel scanning of the generatrixes with opposite probes. The implemented strategy consists of four steps as shown in Fig. 11. First, the extraction step, defined above, identifies the three simple elements of the cylindricity. The extracted surface results from the combination of the identified elements. In step 2, the cylindrical surface is obtained by filtering the extracted surface using an appropriate filter (FFT, Gaussian or spline filters), and validated least squares fitting or Chebyshev best-fit based on Small Displacement Torsor methods ([19]) is applied in step 3. In the final step 4, local deviations are estimated and the cylindricity parameters are calculated while computing the peak-to-valley deviations.

5. Experiment and discussion

The experiment aims at calibrating a high quality cylinder of 300 mm diameter inside a cleanroom where the temperature and humidity are controlled to 20 °C ± 0.3 °C and 50 ± 5 %, respectively. The measurement protocol was applied according to the following five steps. (i) Each measuring and reference capacitive probe is in-situ calibrated, with two opposite laser interferometers, to residual non-linearity errors below 5 nm. (ii) The centring and tilting of the CP-axis along the rotational axis of the NanoCyl is performed by the automated tilt/centre table. (iii) A set of nine cross-sectional profiles of the CP are obtained by applying the revisited reversal error separation technique. For each circularity profile and angular position of the cylinder, the recording is repeated for $N_c = 6$ cycles. (*iv*) the CP median line deviations are calculated from the first harmonic of the DMT signal including the cylinder and reference probes recordings. (v) The radial deviations $r_d(z)$ are evaluated by a set of 32 generatrixes measurements, performed with opposite probes, each consecutively repeated over three iterations. Furthermore, the whole measurement protocol is repeated four times.

The obtained cross-section circularity profiles and harmonics are shown in Fig. 12. The circularity profiles are harmonic filtered in the

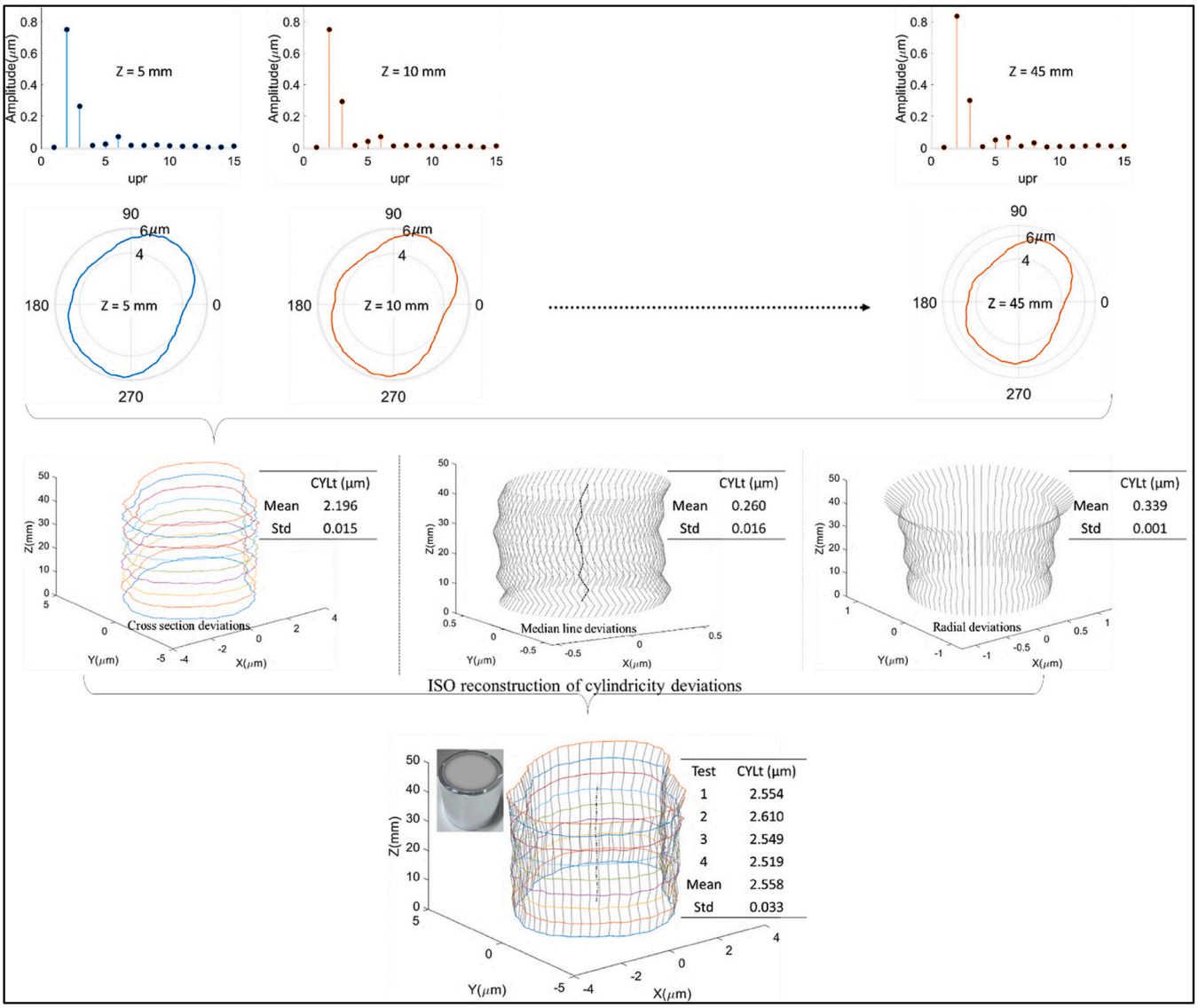

Fig. 12. Cylindricity calibration of the selected high-quality CP including the three simple elements with respect to ISO 12180.

Table 2
Minimum zone circle (MZC) roundness error of cross section circular profiles, its standard deviation (Std) and relative standard deviation (RSD).

Z (mm)	MZC (μm)	Std (nm)	RSD (%)
5	1.892	12.1	0.6
10	1.951	14.3	0.7
15	2.034	4.5	0.2
20	2.093	20.1	1.0
25	2.150	5.8	0.3
30	2.130	15.1	0.7
35	2.068	23.5	1.1
40	2.136	13.2	0.6
45	2.144	21.4	1.0

range [20] undulations per revolution (upr). The Peak-to-valley deviation is determined with the validated Chebyshev best-fit algorithm [17]. The corresponding minimum zone circle (MZC) given in Table 2 shows a maximum relative standard deviation (RSD) of 1.1 %. The extracted cylindrical surface is reconstructed by combining the filtered cross-section circularity profiles, median line and radial deviations. The results, illustrated in Fig. 12, stand for the surface of cylindricity. The obtained mean cylindricity, CYLt, is equal to 2.558 μm, with a standard deviation, Std, of about 33 nm.

6. Error budget and uncertainty estimation

The standard measurement uncertainty depends on the NanoCyl (probes misalignments, CP eccentricity and tilt errors, etc.), environmental conditions (thermal, hygrometry and pressure variations in the cleanroom), measurement process (error separation technique, number N_c cycles, etc.) and data processing (extraction, filtering, association and cylindricity parameters identification (Fig. 11). The probes angular and linear location errors estimated at ~100 μrad and 100 μm, respectively, result from manufacturing and assembly of the machine. The corresponding constant effect is minimised by in-situ calibration below 5 nm (non-linearity residuals).

The first order harmonic effect caused by the CP tilt and eccentricity (~10 μrad and 1.8 μm) is suppressed by calculation, whereas the resulting ovality on the second order is estimated at 0.75 nm. Furthermore, the residual second order effect of the spindle tilt and radial error motion perpendicular to the measurement axis is evaluated at 0.015 nm and 0.33 nm respectively.

The environmental perturbations are reduced by the DMT application and the temperature regulation. In particular the thermal drift effect

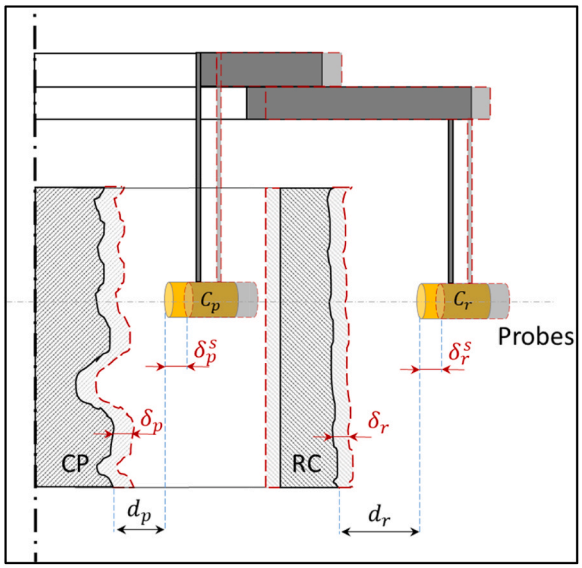

Fig. 13. Schematic of the symmetric configuration of the NanoCyl measuring elements (sensors and carriage structure). The expanded components are represented is red colour. RC=Reference Cylinder.

Table 3
Summary of the standard measurement uncertainty estimation (a_+ is the value of the given error, $e_+$the estimated standard measurement uncertainty).

Error components		a_+ [μrad, μm]	e_+ [nm]
CPs	Tangential spindle error motion		
	B_Y	10	0.33
	γ	100	0.02
	Tilt & Centring		
	Eccentricity	2	0.75
	Tilt	100	0.02
	Indexing errors	350	0.5
Probe	Calibration residuals	0.005	5
Environment	Thermal drift	0.001	1
Data processing	Synchronous/asynchronous separation ($N_c = 6$)	0.047	33.4
Standard measurement uncertainty u			**33.8**

is alleviated by the symmetrical architecture of the metrology frame (Fig. 13). Its estimation under the assumption of axisymmetric expansion is obtained with Eq. (12). The given result is in order of ~1 nm and ~16 nm for a probe measurement range of 115 μm and 2.2 mm respectively.

$$\Delta_{p,r} = \delta^s_{p,r} - \delta_{p,r} = \alpha_{p,r} d_{p,r} \delta T \tag{12}$$

Where $\delta_{p,r}$ are the radial expansion of the cylinders, $\delta^s_{p,r}$ are the radial expansion of the probe carriage stage; $\alpha_{p,r}$ are the thermal expansion coefficients of the cylinders, $d_{p,r}$ are the probes measuring range and δT is the thermal gradient uniformly distributed in the measuring volume.

The errors related to the measurement process derive from the specific operations required during the extraction of cylindricity elements. In particular, imperfect CP repositioning with indexing error estimated at 0.02° when applying the revisited reversal, influences the measurement with an effect evaluated at 0.5 nm. The influence of the main error sources is summarised in Table 3. The combined standard measurement uncertainty is estimated to 33.8 nm. Data processing appears to be the main contributor. In particular, the repeatability of the DMT synchronous data sets are evaluated to ~ 47 nm for $N_c = 6$. This leads to standard deviations for cross-section, radial and median line deviations estimated at ~15 nm, 1 nm and 16 nm, respectively.

Table 4
Evolution of the standard measurement uncertainty with respect to the number of repeated cycles and probe measuring range.

N_c	DMT Synchronous Std (nm)	u (nm) $d_{p,r}$	
		112 μm	2.15 mm
4	57.8	41.2	44.2
6	47.3	33.8	37.4
8	35.3	25.5	30.1
10	9.9	8.7	18.2

Additional experiments were conducted with a larger number of cycles. The results show a more precise separation of DMT synchronous from asynchronous. In particular, for $N_c = 10$, the DMT synchronous Std is reduced to 9.9 nm (Table 4). It leads to a better identification of both the cross-section and the median line deviations with a combined standard measurement uncertainty of 8.7 nm (U (k = 2) = 17.4 nm) under similar measurement conditions. These results demonstrate the capability to perform cylindricity evaluations of CPs with an achievable standard measurement uncertainty of few tens of nanometres.

7. Conclusion

Ultra-high accuracy cylindricity measurement is investigated in accordance with ISO 12180–1. The developed protocol uses the architecture of the ultra-high precision NanoCyl cylindricity-measuring machine, rigorously applying Precision Design Principles (PDPs). It employs a birdcage extraction strategy for the cylindrical surface and identifies the three components of cylindricity deviations step-by-step. Cross-section deviations are isolated through a revisited reversal error separation technique, while median line deviations are evaluated using the first harmonic of the DMT synchronous data. Radial deviations are derived from multiple measurements along parallel generatrixes using opposite capacitive probes. After combining these elements, the cylindrical surface is filtered, and local and global cylindricity parameters are calculated based on an associated reference feature. Results demonstrate the capability to achieve cylindricity assessments with a standard measurement uncertainty of a few tens of nanometres, meeting the stringent demands of advanced manufacturing.

Future work will focus on optimising NanoCyl's spatial redundancy to minimise measurement requirements and developing a hybrid digital twin for uncertainty estimation, prediction, and optimisation. This progress will support advanced manufacturing by enhancing accuracy in high-precision applications and enabling more efficient process control through reliable, nanometre-level quality assessments.

Declaration of Competing Interest

The authors declare that they have no known competing financial interests or personal relationships that could have appeared to influence the work reported in this paper.

Acknowledgements

This work has been carried out within the project 22DIT01 ViDiT and the project 23IND08 DI-Vision, which have received funding from the European Partnership on Metrology, co-financed from the European Union's Horizon Europe Research.

References

[1] Schönemann Lars, et al. Synergistic approaches to ultra-precision high performance cutting. CIRP J Manuf Sci Technol 2020;28:38–51.
[2] Kurita Tsuneo, Kasashima Nagayoshi, Matsumoto Mitsutaka. Development of a vision-based high precision position and orientation measurement system to facilitate automation of workpiece installation in machine tools. CIRP J Manuf Sci Technol 2022;38:509–17.

[3] Schmitz TL, Couey J, Marsh E, Mauntler N, Hughes D. Runout effects in milling: surface finish, surface location error, and stability. Int J Mach Tools Manuf 2007;47 (5):841–51. https://doi.org/10.1016/j.ijmachtools.2006.06.014.
[4] Huo FW, Kang RK, Li Z, Guo DM. Origin, modeling and suppression of grinding marks in ultra precision grinding of silicon wafers. Int J Mach Tools Manuf 2013; 66:54–65. https://doi.org/10.1016/j.ijmachtools.2012.11.006.
[5] R. Henselmans, "Non-contact measurement machine for freeform optics," 2009, doi: ⟨10.6100/IR641380⟩.
[6] ISO 12180-1:2011. Geometrical Product Specifications (GPS) — Cylindricity — Part 1: Vocabulary and Parameters of Cylindrical form. Geneva: ISO,; 2011.
[7] Liu W, Hu P, Fan K. Comparison of current five-point cylindricity error separation techniques. Appl Sci 2018;8(10). Art. no. 10.
[8] Liu W, Fu JS, Wang B, Liu S. Five-point cylindricity error separation technique. Measurement 2019;145:311–22. https://doi.org/10.1016/j.measurement.2019.05.072.
[9] Lee JC, Shimizu Y, Gao W, Oh J, Park CH. Precision evaluation of surface form error of a large-scale roll workpiece on a drum roll lathe. Precis Eng 2014;38(4): 839–48. https://doi.org/10.1016/j.precisioneng.2014.05.001.
[10] Schellekens P, Rosielle N, Vermeulen H, et al. Design for precision: current status and trends. CIRP Ann - Manuf Technol 1998;47(2):557–86.
[11] Yagüe-Fabra JA, Gao W, Archenti A, et al. Scalability of precision design principles for machines and instruments. CIRP Ann - Manuf Technol 2021;70(2):659–80.
[12] Evans CJ, Estler WT, Hocken RJ. Self-calibration: reversal, redundancy, error separation, and 'absolute testing. CIRP Ann - Manuf Technol 1996;45(2):617–34.
[13] Prieto E, Muñoz R, Koops R, et al. High precision roundness measurement by error separation techniques (EURAMET. L-S30). Metrologia 2022;59(1A):04003.
[14] Haitjema H. Revisiting the multi-step method: enhanced error separation and reduced amount of measurements. CIRP Ann - Manuf Technol 2015;64(1):491–4.
[15] Nouira H, Vissiere A, Damak M, David J-M. Investigation of the influence of the main error sources on the capacitive displacement measurements with cylindrical artefacts. Precis Eng 2013;37(3):721–37. https://doi.org/10.1016/j.precisioneng.2013.02.005.
[16] Zhang GX. A study on the Abbe principle and Abbe error. CIRP Ann - Manuf Technol 1989;38(1):525–8.
[17] Bouderbala K, Nouira H, Girault M, et al. Effects of thermal drifts on the calibration of capacitive displacement probes at the nanometer level of accuracy. IEEE Trans Instrum Meas 2015;64(11):3062–74.
[18] Marsh ER. Precision Spindle Metrology. Lancaster, PA: DEStech Publications, Inc.,; 2008. ISBN: 978-1-932078-77-0.
[19] Clement A, Bourdet P. A study of optimal-criteria identification based on the small-displacement screw model. CIRP Ann - Manuf Technol 1988;37(1):503–6.